

KEK Preprint 96-7
April 1996
H

Beam tests of a double-sided silicon strip detector with fast binary readout electronics before and after proton-irradiation

Y. Unno^a, M. Takahata^h, H. Maeohmichi^h, F. Hinode^a, T. Akagi^a, T. Aso^b, M. Daigo^c, J. DeWitt^d, D. Dorfand^d, T. Dubbs^d, M. Frautschi^e, A. Grillo^d, C. Haber^f, T. Handa^g, T. Hatakenaka^h, B. Hubbard^d, H. Iwasaki^a, Y. Iwata^g, D. Kaplanⁱ, S. Kashigin^d, I. Kipnis^f, S. Kobayashij, T. Kohriki^a, T. Kondo^a, W. Kroeger^d, J. Matthews^k, H. Miyata^b, A. Murakamij, K. Noble^d, K. O'Shaughnessy^d, T. Ohmoto^g, T. Ohsugi^g, H. Ohyama^g, T. Pulliam^d, J. Rahn^d, W.A. Rowe^d, H.F.-W. Sadrozinski^d, A. Seiden^d, J. Siegrist^f, E. Spencer^d, H. Spieler^f, R. Takashima^l, N. Tamura^h, S. Terada^a, M. Tezukaj, A. Webster^d, R. Wichmann^d, M. Wilder^d, M. Yoshikawa^g

^a Department of Physics, KEK, Tsukuba, Ibaraki 305, Japan

^b Department of Physics, Niigata University, Niigata 950-21, Japan

^c Department of Economics, Toyama University, Toyama 930, Japan

^d SCIPP, University of California, Santa Cruz, CA 95064, USA

^e Department of Physics, Texas Tech University, Lubbock, TX 79409-1051, USA

^f Department of Physics, LBNL, Berkeley, CA 94720, USA

^g Department of Physics, Hiroshima University, Higashi-Hiroshima 724, Japan

^h Department of Physics, Okayama University, Okayama 700, Japan

ⁱ Department of Physics, University of Oklahoma, Norman, OK 73019, USA

^j Department of Physics, Saga University, Saga 840, Japan

^k Department of Physics, University of New Mexico, Albuquerque, NM 87131, USA



SW9625

Presented at the 2nd International Symposium on Development and Application of Semiconductor Tracking Detectors, at Hiroshima, Oct. 10-13, 1995, and to be published in Nucl. Instr. Meth.

National Laboratory for High Energy Physics, 1996

KEK Reports are available from:

Technical Information & Library
National Laboratory for High Energy Physics
1-1 Oho, Tsukuba-shi
Ibaraki-ken, 305
JAPAN

Phone: 0298-64-5136
Telex: 3652-534 (Domestic)
(0)3652-534 (International)
Fax: 0298-64-4604
Cable: KEK OHO
E-mail: Library@kekvox.kek.jp (Internet Address)
Internet: <http://www.kek.jp>

Beam tests of a double-sided silicon strip detector with fast binary readout electronics before and after proton-irradiation

Y. Unno^a, M. Takahata^h, H. Maeohmichi^h, F. Hinode^a, T. Akagi^a, T. Aso^b, M. Daigo^c, J. DeWitt^d, D. Dorfan^d, T. Dubbs^d, M. Frautschi^e, A. Grillo^d, C. Haber^f, T. Handa^g, T. Hatakenaka^h, B. Hubbard^d, H. Iwasaki^a, Y. Iwata^g, D. Kaplanⁱ, S. Kashigin^d, I. Kipnis^f, S. Kobayashi^j, T. Kohriki^a, T. Kondo^a, W. Kroeger^d, J. Matthews^k, H. Miyata^b, A. Murakami^j, K. Noble^d, K. O'Shaughnessy^d, T. Ohmoto^g, T. Ohsugi^g, H. Ohyama^g, T. Pulliam^d, J. Rahn^d, W.A. Rowe^d, H.F.-W. Sadrozinski^d, A. Seiden^d, J. Siegrist^f, E. Spencer^d, H. Spieler^f, R. Takashima^l, N. Tamura^h, S. Terada^a, M. Tezukaj, A. Webster^d, R. Wichmann^d, M. Wilder^d, M. Yoshikawa^g

^a Department of Physics, KEK, Tsukuba, Ibaraki 305, Japan

^b Department of Physics, Niigata University, Niigata 950-21, Japan

^c Department of Economics, Toyama University, Toyama 930, Japan

^d SCIPP, University of California, Santa Cruz, CA 95064, USA

^e Department of Physics, Texas Tech University, Lubbock, TX 79409-1051, USA

^f Department of Physics, LBNL, Berkeley, CA 94720, USA

^g Department of Physics, Hiroshima University, Higashi-Hiroshima 724, Japan

^h Department of Physics, Okayama University, Okayama 700, Japan

ⁱ Department of Physics, University of Oklahoma, Norman, OK 73019, USA

^j Department of Physics, Saga University, Saga 840, Japan

^k Department of Physics, University of New Mexico, Albuquerque, NM 87131, USA

^l Department of Education, Kyoto University of Education, Kyoto 612, Japan

A double-sided silicon strip detector with a radiation-tolerant design was fabricated and characterized in a sequence of beam tests at KEK using 4 GeV/c pions. The detectors were combined with newly designed, fast, lower power, bipolar amplifier-shaper-discriminator chips and CMOS digital pipeline chips to record hit-no hit signals in the strips. Efficiencies, noise occupancies, and spatial resolutions were measured before and after the proton irradiation at an equivalent fluence of 1×10^{14} p/cm², depending on angle of track incidence and strip-pitches. The median pulse height distribution, derived from the threshold scans of the efficiency, allowed to extract the response of the detector. A 1 Tesla magnetic field enabled us to determine the Hall mobilities of electrons and holes.

1. Introduction

Silicon strip detectors have been proposed to be used as a precision tracking and vertexing device in high-energy-physics experiments^[1]. In future experiments, such as ATLAS^[2] at the LHC^[3], one major concern is the tolerance of silicon detectors to the high radiation environment. The ATLAS silicon strip detector anticipates a cumulative fluence of more than 10^{14} charged particles/cm² over a lifetime of 10 years.

A number of studies have been performed to understand the radiation effect to the silicon strip detectors^[4] and a double-sided silicon strip detector (DSSD) has been produced with a radiation tolerant design^[5]. The latest specification of the design is summarized in Table 1. The silicon bulk was the n-type and the axial strips were processed in the n-side, and the stereo strips (10 mrad stereo-angle) in the p-side, with a strip pitch of 50 μ m. The implant strips were AC-coupled to aluminum readout-electrodes, via sandwiched thin SiO₂ and SiN insulators. A goal of the design was to operate the detector at a bias voltage of up to 200 V, while grounding the readout electrodes, before and after the type inversion of the silicon bulk due to the radiation damage.

Simple, fast, and low-power electronics were developed to read out the strip detectors^[6]. High speed was required to tag an event to the bunch crossing and to keep the occupancy low. The bunch crossing frequency at the LHC will be 40 MHz. Low power was required to make the cooling of a large system manageable. The ATLAS system will have several million channels. The readout scheme was a simple "Binary-readout" that registered only hit and no-hit information in a channel for the pulse height above a threshold. The one-bit of data was stored in a digital pipeline until a trigger arrived.

Along with developing a radiation-tolerant silicon strip detector, understanding of the detector response before and after radiation damage was an urgent task. A combination of the DSSD and the binary readout electronics was beam-tested at KEK using 4 GeV pions from its 12 GeV proton synchrotron, for proof of principle, and subsequently, for characterization of improved versions before (T280, T330) and after irradiation (T355) ^[7]. The DSSD was irradiated with protons at TRIUMF and at LBNL.

In previous reports^[8, 9], we have presented the responses of the non-irradiated and irradiated detectors mainly to normal incident particles. In the ATLAS layout of the silicon tracking system, charged tracks of 1 GeV/c momentum hit the detector at an angle of 10° at a radius of 60 cm perpendicular to the

axial strips because of the 2 Tesla magnetic field, in addition to a tilt angle of the detectors. The charges, i.e., electron and hole pairs, generated along a track in the silicon bulk, will split into two or more strips due to the inclination and the magnetic field. This charge sharing may lead to inefficiency depending on the angle and the threshold of the binary electronics.

The detector-under-test (DUT) had a basic readout pitch of 50 μm . A readout region was arranged by ganging to have readout pitches of 100 μm and 150 μm in order to evaluate the response to other pitch configurations. In this report, we will describe dependence of the responses of the DSSD with the fast binary readout electronics to the angles of track incidence and the pitch configurations.

Table 1
Specification of the radiation-hard double-sided silicon strip detector. Two fabrications: DSSD1 with the standard implant-process parameters and DSSD2 with an improvement^b.

(1) Substrate	
Type	n-type Si
Resistivity	4–8 k Ω -cm
Thickness	300 \pm 10 μm
(2) Size	
Overall dimension ^a	60 mm \times 34.1 mm
Stereo-effective area	58.8 mm \times 31.4 mm
(3) Strip	
Axial strips	n-side
Stereo strips	p-side
Pitch	50 μm
Stereo angle	10 mrad
Implant width	12 μm
Implant depth	>1 μm and round edge ^b
AC electrode width	<10 μm
Strip isolation on n-side	common p-implant
(4) AC coupling	
Insulator	SiO ₂ +SiN
(5) Bias resistor	
Polycrystalline silicon	250 \pm 50 k Ω

^a Actual dimension is 60 μm narrower due to sawing

^b This is for the DSSD2.

2. Experiment

2.1. Setup

Three beam tests, T280, T330, and T355, were set up at the $\pi 2$ test beam line of the 12-GeV proton synchrotron at KEK. Three scintillation counters, S_1 , S_2 , S_3 , were set upstream of the detectors to make a trigger for 4 GeV negative pions initiating a data-acquisition sequence. The S_1 , S_2 , and S_3 had a size of 2 cm (width) \times 2 cm (height) \times 5 mm (thickness). S_2 and S_3 were placed close together but displaced from the beam centerline with respect to each other to make a smaller overlapping region: 2 cm \times 1 cm by displacing vertically or 1 cm \times 1 cm by displacing diagonally. S_1 was set 3 to 4 m upstream and the S_2 \cdot S_3 pair at about 1 m upstream of the

detectors. Two additional small counters, F_1 and F_2 , slightly wider than the readout area, were placed in front of and behind the detectors, for limiting the trigger area, checking the alignment of the detectors and the consistency of the counts in the counters and the detectors, etc. The F_1 and F_2 counters were read out with optical fibers to allow their placement in a magnetic field. Two Cerenkov counters were used occasionally to differentiate pions and electrons (the fraction of electrons was a few % of the total particles). The coordinate system defined was right-handed: +z in the beam-direction and +y in the upward direction.

The silicon strip detectors were placed on a translation-rotation stage inside an aluminum box. The box, of dimensions 60 cm (width) \times 39 cm (height) \times 65 cm (depth), shielded the detectors electrically and optically and made a cooled environment for the electronics with an forced air flow. The translation-rotation stage was set in the box to move the detectors in the x-direction, rotate in ϕ around the y-axis, and rotate in θ around the rotated x-axis. The direction of the detector axial strips was vertical. For the ϕ angle rotations, two methods were employed: for small rotations, only the stage was rotated (Fig. 1(A)); for larger rotations the detectors were stepped with extra fixtures in addition to the rotations since the readout region was limited (Fig. 1(B)). In T280, a vertical magnetic field of up to 1.0 Tesla was provided (direction towards -y) by a dipole magnet (USHIWAKA) which had an opening aperture of 82 cm(W) \times 40 cm(H) \times 70 cm(D).

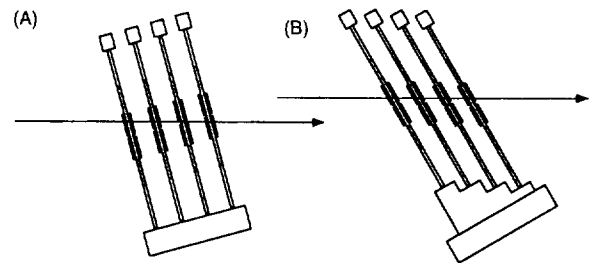


Fig. 1 Rotation schemes: (A) rotation of the stage for a small rotation angles, (B) with extra stepping fixtures for larger rotation angles. Several types of the stepping fixtures were prepared for different angles.

Three planes of detectors in T280 and four planes in T330 and T355 were set and aligned in a mini-crate on the translation-rotation stage. A schematic presentation of a setting is shown in Fig. 2. The detector planes were separated by 8 mm to minimize the multiple-scattering effect. For 4 GeV/c pions, the r.m.s. deviation of the hit in the middle plane from the straight line connecting the hits in the adjacent planes was calculated to be 0.3 μm due to the 300 μm silicon material in the middle plane.

The most-upstream and the most-downstream silicon detectors were the anchors and the inner two detectors were the detector-under-test (DUT). The anchor and the DUT detectors used the same double-sided silicon strip detectors whose spec is summarized in Table 1. The anchor detectors

had an identical strip-pitch arrangement and were non-irradiated. The first DUT (DUT1) was the one tested before and after proton irradiation, and having several strip-pitch configurations as described in the following section. Out of the two DUT's (DUT1 and DUT2) in runs T330 and T355, only the results for DUT1 are presented in this report.

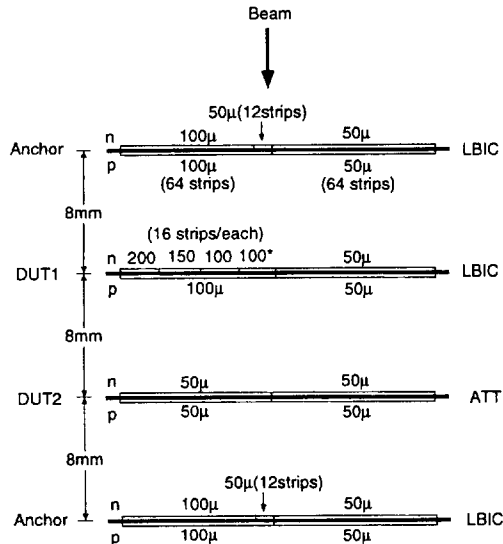


Fig. 2 Detector setup of T330 and T355. The n-side had the axial strips and the p-side the stereo strips (10 mrad. stereo angle).

The front-end electronics (FEE) consisted of pairs of chips: a bipolar amplifier-shaper-discriminator chip, and a CMOS digital pipeline chip (CDP64) clocked at 10 or 40 MHz [10]. Three different bipolar amplifier-shaper-comparator chips were used: TEKZ, LBIC and ATT, all of which had unipolar Poisson/Gaussian shaping circuitry. The TEKZ chip had a slow peaking time of 30 ns [11]. The LBIC chip had a fast 22 ns shaping meant for the 40 MHz operation [6] and was fabricated on the DUT1. The ATT chip had a slower peaking time but had time-walk compensation circuitry to improve the time resolution [12] and on the DUT2. Due to a two-level buffering scheme in the digital pipeline chips driven by a clock pulse, the analog signal processing and the digital buffering in the pipeline functioned simultaneously. The existence or non-existence of clock pickup by the analog chip was one of the issues of the beam test. Only the central 128 channels on both sides of all detectors (6.4 mm width), requiring two pairs of 64 channel FEEs, were instrumented. The detector strip length connected was 6 cm. The setups used for three runs are summarized in Table 2.

A schematic drawing of the detector-electronics chain is presented in Fig. 3. The detector is symbolically drawn by the diode. In the detector and binary-readout electronics, performance can be controlled by two parameters: a detector bias voltage for depleting the detector, and a threshold of the discriminator for limiting the noise occupancy and for the hit-no hit counting. Analog information was obtained by scanning the threshold.

Table 2
A summary of the beam test setups

	Number of detectors	Detector type	Front-end Electronics	Clock [MHz]	Rotation stage
T280	3	DSSD1	TEKZ	10	(A)
T330	4	Non-irrad-DSSD2	LBIC, ATT	40	(B)
T355	4	Irrad-DSSD2	LBIC, ATT	40	(B)

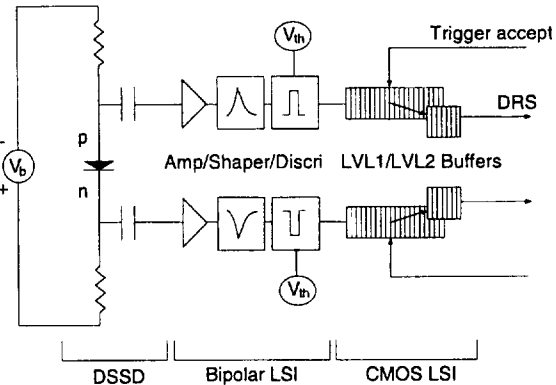


Fig. 3 Schematic representation of the DSSD and binary FEE chain. There are two parameters to control the chain: the bias voltage and the threshold of the discriminator.

2.2. Data Acquisition

The data acquisition (DAQ) was done using a VME-UNIX DAQ system (UNIDAQ) [13]. A UNIX workstation (DEC station 5000/125) communicated with VME modules through the DEC Turbo-channel VME adapter in the workstation and the DEC PMABV-T6000-AA VME module in a VME crate. CAMAC modules were communicated via VME.

The communication between VME and the FEE on the detector was made through a VME module called the digital readout sequencer (DRS) [14]. The DRS also received clock, threshold voltage, and calibration signals and routed them to the detectors. The difference (in time) of a trigger and the clock was measured with a CAMAC TDC.

2.3. Ganging of Detector Strips

To characterize the detector performance as a function of strip-pitch, the detector strips were wire-bonded to the FEE channels in several configurations. In the anchor detectors, the strips in one chip set were bonded successively to the individual FEE channels with the 50 μm pitch. In the other chip set, two strips were ganged into one FEE channel, giving an effective 100 μm pitch. In the DUT1, the p-side had the same configuration with the anchors. In the n-side, the chip sets were bonded using five different configurations: one chip set was bonded successively to individual channels (50 μm); the other chip set with, alternate bonding with intermediate strips unbonded, thus giving a case of one intermediate

floating-strip readout ($100^* \mu\text{m}$), two adjacent strips being ganged into one channel ($100 \mu\text{m}$), three strips into one channel ($150 \mu\text{m}$), and four strips into one channel ($200 \mu\text{m}$). A small region of the n-side $100 \mu\text{m}$ region of the anchor detectors was bonded fully to give a $50 \mu\text{m}$ configuration to cover the DUT1 $100^* \mu\text{m}$ region with the $50 \mu\text{m}$ anchor configuration.

The connection of the detector strips and the electronics channels are shown graphically in Fig. 4. The case classifications of the DUT and the anchor pitches are summarized in Table 3. Although subtleties such as the electric field lines, input capacitance of a channel, are different between the ganged-strip pitches and wide-spacing single-strip pitches, the performance of these configurations should be a good guideline for different strip pitches.

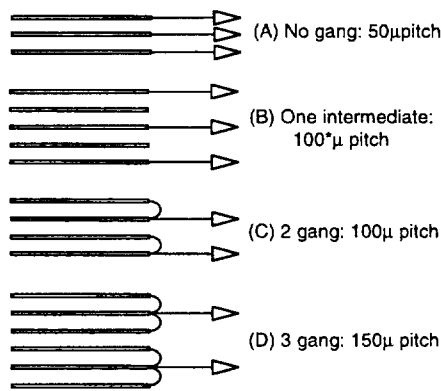


Fig. 4 Graphical representation of the ganging of detector strips into FEE channels (triangle) on the n-side of DUT1 in T330 and T355.

Table 3
Ganging-case classification

Case	Ganging	DUT Pitch [μm]	Anchor pitch [μm]
$50 \mu\text{m}$	No	50	50
$100^* \mu\text{m}$	One-intermediate	100	50
$100 \mu\text{m}$	2	100	100
$150 \mu\text{m}$	3	150	100
$200 \mu\text{m}$	4	200	100

2.4. Proton Irradiation

The DUT1 of the T330 run was irradiated with protons at TRIUMF and at LBNL. The fluence at TRIUMF was below 10^{13} p/cm^2 . The LBNL irradiation had a spot which was 1.5 cm in diameter at its peak. The maximum fluence in the instrumented area was estimated to be $4.6 \times 10^{13} \text{ p/cm}^2$. In order to get a higher equivalent damage, the DUT was warmed up to expedite anti-annealing; the expected damage level at the time of the beam test (T355) was estimated to be equivalent to a fluence of $1 \times 10^{14} \text{ p/cm}^2$ in terms of depletion voltage (120 V estimated). Since the spot was much smaller than the detector size ($6 \text{ cm} \times 3.4 \text{ cm}$), the fluence along the instrumented strips was not uniform: over the 6 cm strip, the

peak of the fluence was at $y \sim 4.2 \text{ cm}$ where the bulk type was inverted (from the initial n-type to p-type), whereas at $y \sim 1.5 \text{ cm}$, the effective doping level dropped to zero, i.e., intrinsic. Details of the proton irradiation and the fluence profile can be found in the ref. 9.

2.5. Data Summary

Parameters varied in the three beam tests were: (1) the bias voltage, (2) the threshold, (3) the incident angles in the ϕ and θ directions where the ϕ direction was the angle perpendicular to the strip directions, (4) the magnetic field. In the T280 run, the incident angles and the magnetic field were varied, and in T330 and T355, the bias voltage, threshold, and ϕ angles were varied. There was no magnetic field in those two tests. The range of variations are summarized in Table 4. The parameter variation was diagonalized most of the time, i.e., only one parameter was varied at a time. The T280 and T330 data were for non-irradiated detectors, and the T355 data for the irradiated detector.

Table 4
Summary of the data taken in T280, T330, and T355

	Bias voltage [V]	Threshold [fC]	Incident angles ϕ [$^\circ$]	θ [$^\circ$]	Magnetic field [T]
T280	100	^a 1.2/0-6	0-9	0-54	0,1
T330	60-120	0-2	0-54	0	0
T355	40-160	0-6	0-45	0	0

^a Mostly at 1.2 fC

3. Results

3.1. Irradiated Detector

In the binary electronics, the observable quantity is the number of signals above a threshold. In a physics experiment the threshold will be kept at a constant value for most of the experimental time. Two important issues in the beam tests were: (1) the efficiency of the system at thresholds characteristic of a physics experiment, and (2) the signal and noise behavior needed to determine the head-room of the system. Issue (1) can be addressed directly in the beam test. Issue (2) can be studied, even with binary electronics, by scanning the threshold.

The efficiency variation as a function of threshold is shown in Fig. 5(a) for DUT1, on the n-side at the most highly irradiated point ($y = 4.2 \text{ cm}$) at a bias voltage of 120V for normally incident pions. The efficiency was defined by the existence of a hit within a window (\pm three $50 \mu\text{m}$ -strips) around the interpolated point from the upstream and the downstream anchor hits or clusters. The cluster was defined when the hit strips were consecutive; the cluster-center was the geometrical center of the hit strips in a cluster. Only one cluster was allowed in each anchor plane. Below a threshold value of 1.5 fC the efficiencies were essentially 100%. Above

1.5 fC, the efficiency started to decrease and reached 50% at 3.0 fC (50 μm pitch) and 3.5 fC ($\geq 100 \mu\text{m}$ pitch). The 50% point is the median pulse height of the energy deposition (Landau distribution). The observation was consistent with the lower tail of the Landau distribution is at about half of the median pulse height.

The electronic noise behavior can be expressed by occupancy, i.e., the noise hit rate of a single strip. The occupancy was evaluated for the strips more than \pm six 50 μm -strips away from the interpolated track points, and is shown in Fig. 5(b) as a function of the threshold. There were two components in the distribution: (1) the intrinsic electronic noise which was increasing exponentially below 1 fC, and (2) the nearly flat distribution above 1 fC at a level of 10^{-4} . The source of this flat distribution is yet to be identified. The occupancy in the sampling before the actual trigger showed an ideal fall-off of the intrinsic noise down to 10^{-6} at thresholds above 1 fC. This indicated that the source of the noise was correlated with the hits by beam particles triggered. It should be pointed out that the detector strip length of the beam tests was 6 cm, while in ATLAS 12 cm in length will be used.

A scatter plot of the efficiency vs. noise occupancy is shown in Fig. 6. Each point represents a threshold setting. The sudden break-off at the efficiency near 100% and the occupancy at about 10^{-4} is a reflection of high efficiency and low intrinsic-noise occupancy.

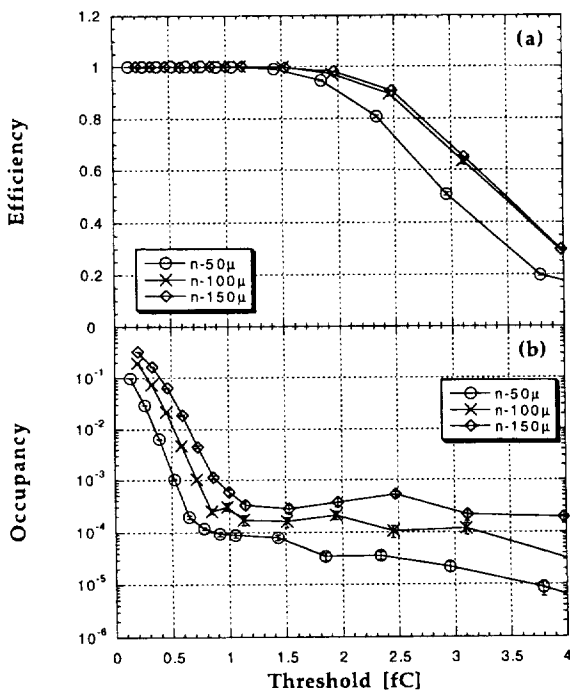


Fig. 5 (a) Efficiency and (b) occupancy as a function of threshold for the normal incident pions. The data were collected for the n-side of the irradiated DUT1 at $y = 4.2$ cm and at a bias voltage of 120V. Responses of three pitches are shown: 50 μm (circle), 100 μm (cross), and 150 μm (diamond).

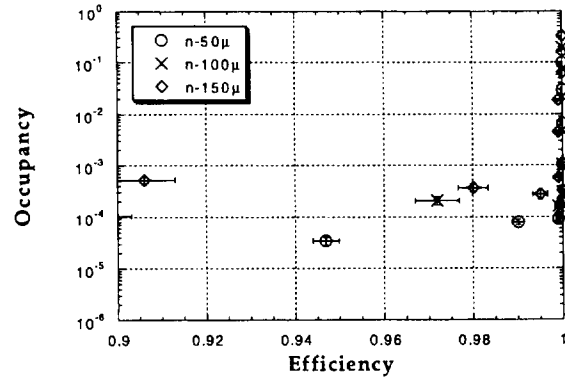


Fig. 6 Efficiency vs. noise occupancy in the irradiated DUT1 at $y = 4.2$ cm and at a bias voltage of 120V in the n-side: 50 μm (circle), 100 μm (cross), 150 μm (diamond).

The bias dependence of the efficiency is shown in Fig. 7(a) for the most highly irradiated point where the detector was inverted. The threshold was fixed at 1 fC and the bias voltage was varied from 20 to 150V. The efficiency for the n-side was high, while that of the p-side was low. This was a clear indication that the p-n junction was on the n-side. There was little difference in the efficiency for the different effective pitches on the n-side, but a large difference on the p-side.

This behavior can be understood from the median pulse height distribution shown in Fig. 7(b). The 50% efficiency points were obtained by fitting the error function, i.e., the integral of Gaussian distribution, to the threshold scan of efficiency at the bias voltages. Apart from the observation that the wider pitches collected more charges than the 50 μm pitch, the n-side median pulse heights were saturating above 120V, and decreased only slowly with decreasing bias voltage. The p-side median pulse heights were much smaller and decreased rapidly from much higher bias voltages. These can be explained if the bulk were inverted from n-type to p-type. The variation of the n-side median pulse height is well explained by the variation of the depletion depth in the bulk in the bias voltages below 120 V which is proportional to a square-root of bias voltage.

Since the lower end of the Landau distribution is at half of the median signal value, signals for all pitches were essentially above 1 fC on the n-side, even at 40 V. There should be little difference in the efficiency in the 50 μm , 100 μm and 150 μm pitches. For the p-side, the signals were small and the large difference in the pulse height caused the large difference in the efficiency.

The data showed that a pulse height difference on the n-side for the 50 μm pitch and the pitches over 100 μm was more than 10%. The systematic error in the calibration of the absolute charge was estimated to be in a range of 5%. Part of the difference was understood with a signal simulation program^[15] which included: (1) the effect of inducing the charges in the readout strips by the movement of the electrons and holes, and (2) a ballistic deficit by a fast shaping amplifier. The program explained the pulse height difference of about 3%. The rest could be explained by the charge

spread due to a capacitive coupling between the strips (i.e., interstrip capacitance), which is not implemented in the simulation version used here. There was a larger charge spread in the p-side in the partially depletion voltages where the undepleted region spread between the readout strips and the depleted region in the bulk. A further comparison of the non-irradiated and the irradiated DUT1 can be found in the ref. 9.

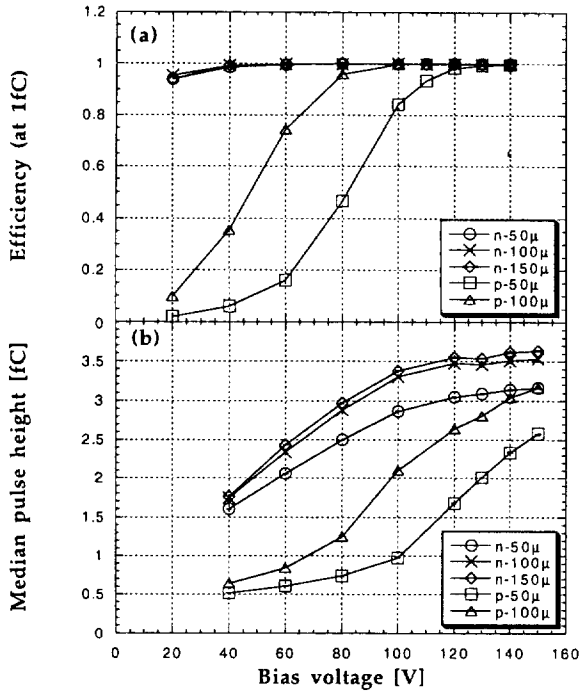


Fig. 7 (a) Efficiency at a threshold of 1 fC and (b) the median pulse height distribution as a function of bias voltage for the normal incident pions. The data was collected for the irradiated DUT1 at $y = 4.2$ cm: 50 μm (circle), 100 μm (cross), 150 μm (diamond) in the n-side; 50 μm (square) and 100 μm (triangle) in the p-side.

3.2. Angular Dependence

3.2.1. Efficiency

When particles hit the silicon strip detector at an angle ϕ (the ϕ incident angle being perpendicular to the strips), the generated electron-holes pairs can be shared between regions sensitive to different strips. This leads to less collected charge per strip and, depending on the threshold, inefficiency.

The angular dependence of the efficiency at the 1 fC threshold of the non-irradiated DUT1 is shown in Fig. 8: (a) for the n-side, and (b) for the p-side at a bias voltage of 100 V, which was about 30 V above the depletion voltage. The 50 μm pitch was fully efficient above 20° and the pitches over 100 μm above 35°. The n-side was slightly less efficient at larger angles than the p-side. The angular dependence of the irradiated DUT is shown in Fig. 9(a) and (b), at 120 V, which was approximately the depletion voltage. The n-side was highly efficient in this case. On the p-side, the 50 μm pitch

showed a large inefficiency. The 100 μm pitch was, on the contrary, fully efficient.

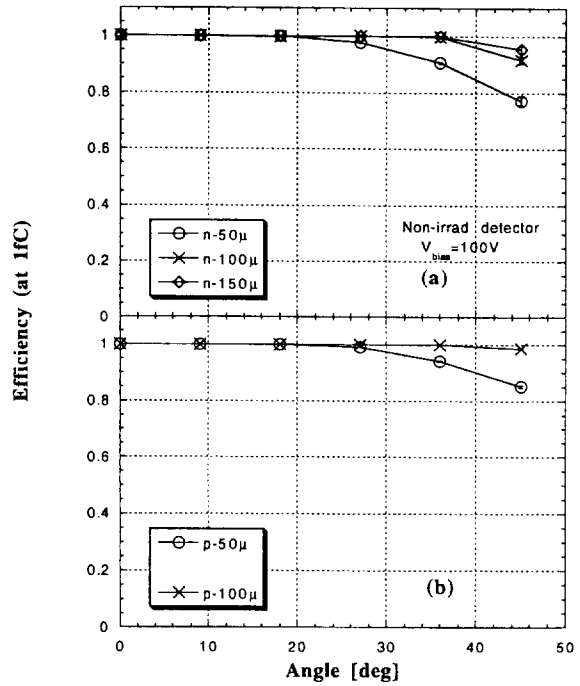


Fig. 8 Angular dependence of the efficiency at a threshold of 1 fC for the non-irradiated DUT1 at a bias voltage of 100V: (a) for the n-side: 50 μm (circle), 100 μm (cross), 150 μm (diamond) pitches; (b) for the p-side: 50 μm (circle), 100 μm (cross) pitches.

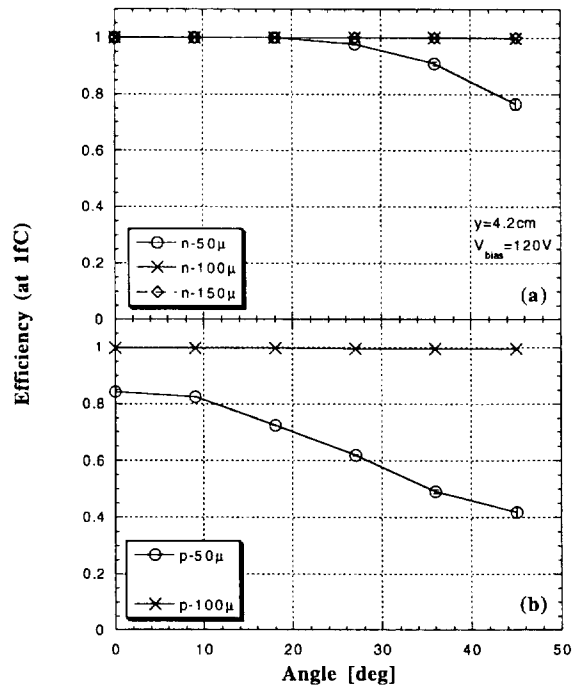


Fig. 9 Angular dependence of the efficiency at a threshold of 1 fC for the irradiated DUT1 at a bias voltage of 120V at $y = 4.2$ cm: (a) for the n-side: 50 μm (circle), 100 μm (cross), 150 μm (diamond) pitches; (b) for the p-side: 50 μm (circle), 100 μm (cross) pitches.

The behavior of the irradiated detector can be understood from the angular dependence of the median pulse height shown in Fig. 10. For the n-side, the median pulse height decreased as the incident angle increased. The larger pitches (100 μm and 150 μm) showed a smaller slope than that of the 50 μm pitch. The effect was a combination of: (1) geometrical, i.e., an increase of the length in angle and a sharing of a track length between the strips, (2) charge spread as observed in Fig. 7(b), and (3) a less depth in case of partial depletion. For the larger pitches, sharing of the charge over fewer strips gave the smaller slopes. On the p-side, the angular dependence was much smaller due to larger effects of (2) and (3). The efficiency plot shows little loss as long as the median pulse height was above 2 fC for a threshold of 1 fC.

In the case of partial depletion, the signal will be lost due to the reduced depletion depth. The angular dependence of the efficiency can be estimated by combining the Fig. 7(b) and the Fig. 10. As described in the introduction, in ATLAS a particle of 1 GeV/c momentum will hit the silicon strip detectors at an incident angle of 10° at the radius of 60 cm. There will be two more angles: (1) the tilt angle of the detector, e.g., 7° , (2) Hall angle of 15.7° in the n-side by the 2 Tesla magnetic field, derived from the measurement in the section 3.4. The 50 μm pitch is fully efficient as long as the tilt angle is made to partially cancel the Hall angle; the 100 μm pitch is fully efficient even when the detector is below full depletion.

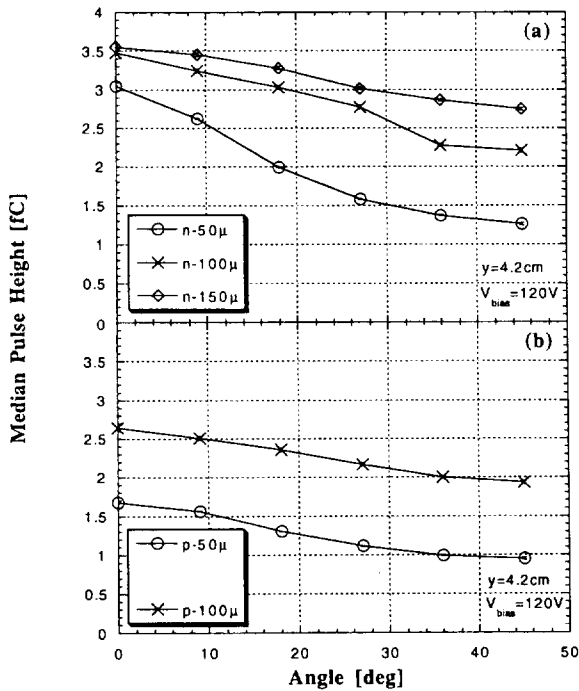


Fig. 10 Angular dependence of the median pulse height of the irradiated DUT1 at the bias voltage of 120V at $y = 4.2 \text{ cm}$: (a) for the n-side: 50 μm (circle), 100 μm (cross), 150 μm (diamond) pitches; (b) for the p-side: 50 μm (circle), 100 μm (cross) pitches.

3.2.2. Spatial Resolutions

Another fundamental issue for the detector-FEE chain is the spatial resolution of the silicon strip detector. The spatial

resolution was derived from the deviation of the hit or cluster in the DUT from the interpolated position from the upstream and the downstream anchors. The hit or cluster was limited within the efficiency window (\pm three strips) in the DUT. The sigma of the deviation was obtained in two ways: (1) in T330, the r.m.s. of the deviation was calculated successively by eliminating the points which were out of 3 sigma's until the r.m.s. converged, (2) in T355 the sigma was obtained by fitting a Gaussian to the Gaussian-smear (with a small sigma) distribution after eliminating the over 3 sigma points once. The reason to apply these methods was that the deviations were quantized because the hits were quantized in the strip pitches. A straight-forward Gaussian fitting did not work because there were zero's between the quantized points. Method (1) should give a smaller sigma of the two. The difference should be the amount of systematic error involved in the estimation of resolutions.

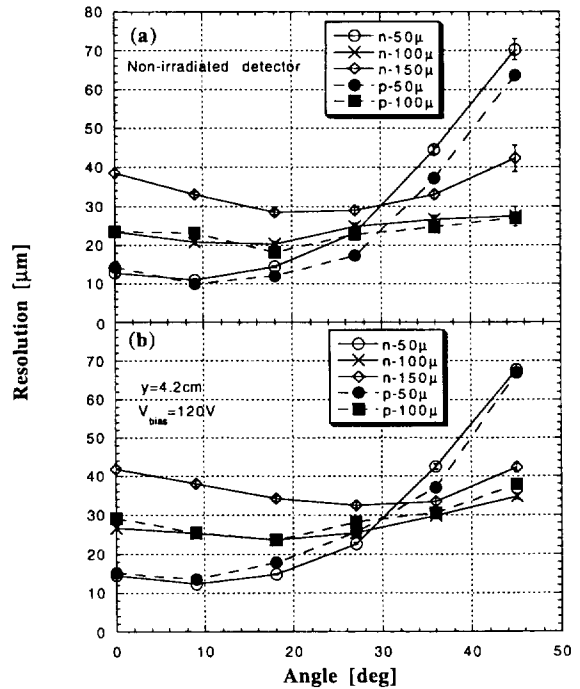


Fig. 11 Spatial resolutions at the threshold of 1 fC: (a) the non-irradiated DUT1 at a bias voltage of 100V, 50 μm (circle), 100 μm (cross), 150 μm (diamond) pitches in the n-side, 50 μm (filled circle), 100 μm (filled square) in the p-side; and (b) the irradiated DUT1 at a bias voltage of 120V and at $y = 4.2 \text{ cm}$, the same designations for the pitches and the marks.

The point spatial resolution was obtained from the deviation sigma as follows. (1) For the regions where the pitches of the DUT and the anchors were same, i.e., in the 50 μm and 100 μm pitches, the point spatial resolution was calculated by multiplying the sigma's with the factor $\sqrt{9/14}$ observed from the triplet distance. The difference of non-irradiated and irradiated detectors was ignored. (2) For the DUT pitches other than 50 and 100 μm , the spatial resolution was obtained by subtracting in quadrature the anchor resolutions obtained in (1) from the sigma's in deviation. The

angular dependence of resulting spatial resolutions of the non-irradiated DUT1 is shown in Fig. 11(a) and those of the irradiated in Fig. 11(b).

The resolutions at the normal incidence were basically consistent with the expected $pitch/\sqrt{12}$ in the non-irradiated and the irradiated cases. In the angular dependence, the minima of the resolutions were observed at the angles of $\tan^{-1}(pitch/thickness)$ where the maximum charge sharing into the adjacent two strips was expected. There was a slight degradation of the resolution in the irradiated data over the non-irradiated one, which source would be the systematic error in the estimation described in the above and/or a real degradation by the radiation damage. The resolutions for the p-side were slightly better than those for the n-side in the non-irradiated while those of the n-side were better than those of the p-side for the irradiated detector. This was consistent with the expectation that the resolution should be better on the side of the p-n junction. The 50 μm pitch resolutions degraded above 20° coinciding with the loss of efficiency above that angle.

In the ATLAS silicon strip detector, the maximum incident angle can be less than 25° and, thus, a detector with any pitch is expected to work. If 90° strips were to be used, e.g., in a vertex layer where a particle will hit at a maximum angle of 50°, a pitch of more than 100 μm is required above an incident angle of 25°.

3.2.3. Effective Spatial Resolution

As seen in Fig. 11, the spatial resolution was improved over the $pitch/\sqrt{12}$ for the tracks at the angle of $\tan^{-1}(pitch/thickness)$. This can be explained by the sharing of charge between two adjacent strips, thus splitting of a "pitch" unit into a single hit and a double hit regions. If the strip pitch (width = P) is split into a single hit region 1 (width = H) and a double hit region 2 (width = W) as shown in Fig. 12, the effective resolution will be, ignoring noise contribution,

$$\begin{aligned} \sigma^2 &= \frac{1}{N} \sum (x - \bar{x})^2 \quad (1) \\ &= \frac{n}{N} \left[\frac{1}{n} \sum (x - \bar{x}_1)^2 \right] + \frac{m}{N} \left[\frac{1}{m} \sum (x - \bar{x}_2)^2 \right] \\ &= \frac{n}{N} \sigma_1^2 + \frac{m}{N} \sigma_2^2 \\ &= \left(\frac{P}{\sqrt{12}} \right)^2 \left[\left(1 - \frac{W}{P} \right)^3 + \left(\frac{W}{P} \right)^3 \right] \quad (2) \end{aligned}$$

where x symbolizes the track position, \bar{x} the center of the hits, n the number of tracks in the region 1, m the number of tracks in the region 2, and N the number of total tracks in the pitch P . The improvement factor is the function of the width W ; the resolution is halved when $W = H = P/2$. The improvement from 14 μm to 12 μm in the 50 μm pitch in Fig. 11 indicated the double-hit width was about $W/P = 10\%$ at the threshold of 1 fC. Although the charges were maximally

shared between two strips in the $\tan^{-1}(pitch/thickness)$ angle case, the threshold of 1 fC was too high to pick up the smaller signals, thus effectively leaving only the narrow region where the charges were split nearly equally for usable charge sharing.

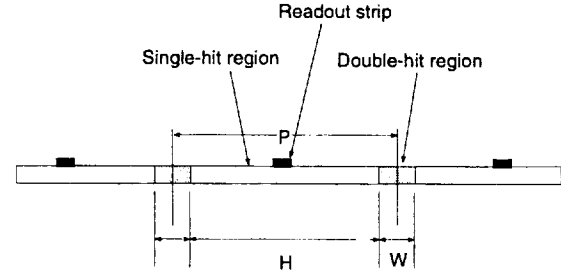


Fig. 12 A schematic drawing of the splitting of a pitch into a single-hit and a double-hit regions.

3.3. Intermediate-floating-strip Readout

3.3.1. Efficiency and Occupancy

One way to create the double-hit region intentionally is to put an extra strip in the middle of the readout strips. This was done in the case of one intermediate floating strips, 100* μm . The intermediate strip had the bias voltage on the implant, thus collecting charges to the strips. Since no amplifier was connected to the readout electrode, the collected charge had to be divided into the neighboring strips, which were grounded or connected to the amplifier (i.e., virtually grounded), according to the interstrip capacitance. In the DUT geometry, where the strips were narrow to reduce the interstrip capacitance, one neighbor would see about 40% of the charge collected in the floating intermediate strips. A real design can be optimized by balancing the maximum coupling to the neighbors and the minimum noise increase by the capacitance. An extreme design of this sort is the charge division readout by inserting more intermediate strips and reading out the amount of charge by analog readout electronics.

The efficiency for the 100* μm case is shown in Fig. 13 as a function of the threshold for the irradiated detector, at $y = 4.2$ cm, a 120V bias voltage, and normally incident pions. The shape of the distribution was quite different from that of no-intermediate case shown in Fig. 5(a). The distribution can be understood to come from the sum of two distributions: the distribution of single-hits in which the median is at around 3 fC (as seen in Fig. 5(a)) and that of double-hits in which the median would be at about 1.2 fC. In the figures, the efficiency reached 100% at a threshold value of 0.7 fC which was a half of the no-intermediate case. The noise occupancy is also shown in the Fig. 13. The occupancy was about equal to that of the 50 μm case.

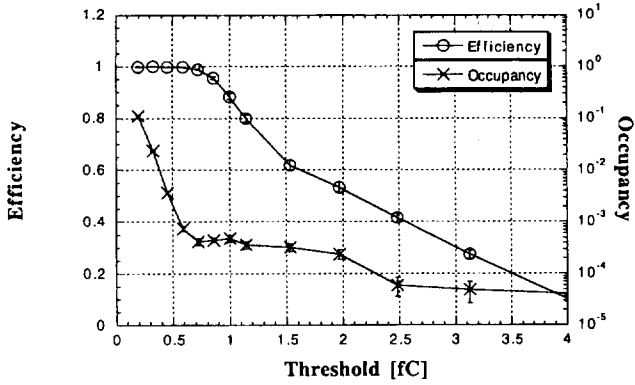


Fig. 13 Efficiency(circle) and noise occupancy(cross) distributions of the 100* μm case in the n-side of the irradiated detector as a function of the threshold at $y = 4.2$ cm and at a bias voltage of 120V for the normal incident pions.

3.3.2. Local Median Pulse Height Distribution

Since the total efficiency was the integral over the single-hit and the double-hit areas, the region for one pitch of the 100* μm case had to be mapped out. The DUT could be measured with a quantization step of 8.3 μm . This was because the pitch of the anchor for the 100* μm case was 50 μm and the quantization in one anchor plane was 25 μm , thus the combination of two anchors in the 1:2 separation ratio to the DUT made the interpolated positions have a step size of 8.3 μm . By binning the efficiency distributions as a function of threshold in the 8.3 μm steps, a local median pulse height distribution was derived as shown in Fig. 14. The unit of the horizontal axis was the 50 μm -pitch strips: the positions 0 and 2 were where the intermediate strips were and the position 1 the readout strips. The offset in the distribution was due to the alignment offset of the anchors and DUT.

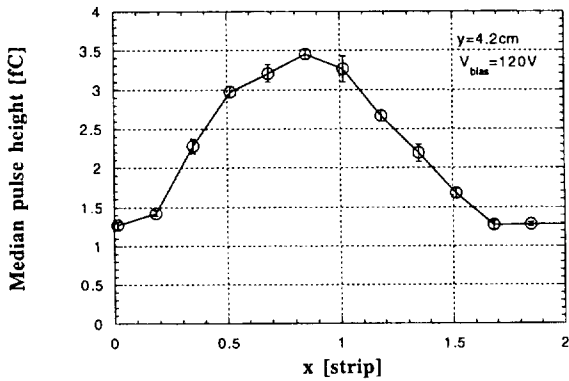


Fig. 14 Local median pulse height distribution in one pitch of the 100* μm case in the n-side of the irradiated detector at $y = 4.2$ cm at a bias voltage of 120V for the normal incident pions.

Two regions were clearly observed: an area of a full charge collection of 3.4 fC at the readout strips and an area of less charge collection, about 1/3 of the full charge, in the intermediate strip regions. The boundary of the regions was smeared out and would be attributed to charge spreading, spatial resolution, and electrical noise contribution. The local

median pulse height distribution confirmed the explanation for the threshold dependence of the efficiency in Fig. 13.

3.3.3. Spatial Resolution

The spatial resolution of the 100* μm case(circle) is plotted in Fig. 15 as a function of the threshold together with that of the no-intermediate strip cases: the 50 μm (cross) and the 100 μm (diamond). Both the 50 μm and the 100 μm cases showed a small improvement in the resolution as the threshold was lowered below 1 fC. This was the effect of picking up a wider double-hit region in the middle of the readout strips. At very low threshold values, the resolution quickly degraded due to the contribution of the intrinsic electronic noise.

The 100* μm case showed a large improvement in the spatial resolution: nearly from the resolution of the 100 μm case at the threshold of 1 fC down to close to that of the 50 μm case at 0.5 fC; much larger than the improvement seen in the no-intermediate 50 μm or 100 μm cases. No further improvement was observed below a threshold level of 0.5 fC because of the noise contribution. Over 1 fC in the 100* μm case, the resolution started to improve again. This was an artificial effect due to the loss of efficiency.

The whole behavior can be understood as follows. When the threshold was very low, the whole pitch, i.e., 100 μm , was sensitive and the spatial resolution would be ideally halved due to the splitting of the single-hit and the double-hit regions. As the threshold was raised, one of the double-hits was lost and the whole pitch became a single-hit region. Thus the spatial resolution reached the value associated with that of the readout pitch. For further threshold increases, both signals in the double-hit region were lost and only the region around the readout strips was sensitive, resulting in the spatial resolution being that of the 50 μm case for the few detected particles.

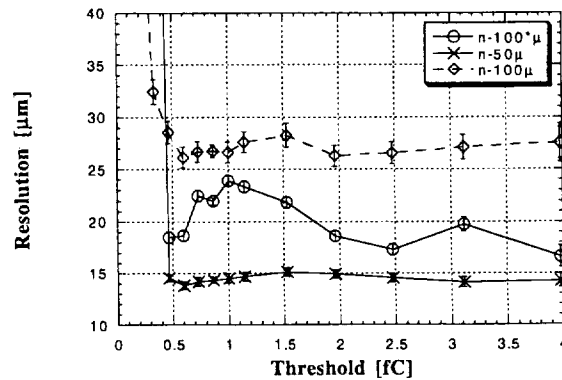


Fig. 15 Spatial resolutions as a function of threshold of the floating-intermediate-readout 100* μm case(circle), the no-intermediate 50 μm (cross), and the 100 μm (diamond) in the n-side of the irradiated detector at $y = 4.2$ cm and at 120V for the normal incident pions.

In the floating-intermediate-strip readout, the improvement of the spatial resolution was limited by the intrinsic noise of the front-end amplifier. Since the pulse height is halved for the hits in the intermediate strips essentially, the threshold has to be halved. There are two ways to improve the situation: (1)

to use an amplifier with lower noise, (2) to add circuitry to suppress the noise; a possibility is given in the appendix.

3.3.4. Angular Dependence of Efficiency and Resolution

The incident angle dependence of the efficiency, etc. was interesting because a segment of a track, which was in the double-hit region for the normal incidence case, would get into the single-hit region because of the inclination, and thus the efficiency would be increased. The efficiency distributions as a function of the incident angle (ϕ angle) are shown in Fig. 16(a) for two thresholds: at 0.6 fC(circle) and at 1.0 fC(cross). The improvement of the efficiency was observed in the 1 fC case: 88% at 0° to >99% around 20° . The corresponding spatial resolutions are shown in Fig. 16(b). The spatial resolution got better where the efficiencies were higher in the angles over 20° . In the 0.6 fC threshold case, the efficiencies were essentially 100%; losing a bit around 20° where the resolutions were slightly worse than those at the higher efficiencies.

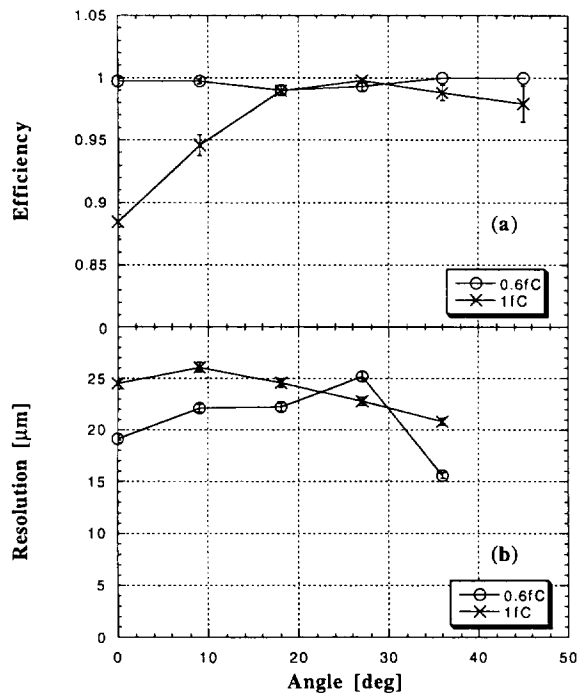


Fig. 16 (a) Efficiencies and (b) spatial resolutions as a function of incident angles for two thresholds: 0.6 fC(circle) and 1.0 fC(cross), in the $100^* \mu\text{m}$ configuration.

3.4. Measurement of Hall Mobility

The swath of electron and hole pairs along the path of charged particles in $300 \mu\text{m}$ thick silicon can be split among several strips by the inclination of incident angles (ϕ -angle) or by the deflection of carriers by a magnetic field (Hall effect). The effect can be observed as a change in the fraction of multiple-strip hits. The distribution of the multi-hit fraction

was measured in the beam test T280 for a non-irradiated detector with and without a magnetic field^[16]. A clear dependence on the incident angle and on the magnetic field was observed as shown in Fig. 17: (a) in the null ($B = 0 \text{ T}$) and (b) in the 1.0 Tesla field ($B = 0.994 \text{ T}$ measured with a NMR meter). The n-side fraction of multiple-strip hits was higher than that of the p-side, possibly because of the combined effect of gain and threshold variation in the electronics and a larger interstrip capacitance found on the n-side.

The ϕ -angle associated with the minimum multiple-strip fraction corresponds to the Hall angle of a carrier and occurs when the Hall effect is canceled out by the incident angle. A hyperbolic function, $y = c\sqrt{1+(x-a)^2/b}$ was fit to the data to extract the minimum. The offset in the ϕ -angle was calibrated using the $B = 0 \text{ T}$ data. From the $B = 1 \text{ T}$ data, the Hall angles (θ_H) for the electrons and the holes were obtained to be $+7.87 \pm 0.24^\circ$ (electrons: n-side) and $-1.85 \pm 0.17^\circ$ (holes: p-side). The corresponding Hall mobilities were $\mu_H^e = 1391 \pm 43 \text{ cm}^2/\text{Vs}$ (electrons) and $\mu_H^h = 325 \pm 30$ (holes) using the relation $\tan\theta_H = 10^{-8}\mu_H B$. The effective dopant concentration of the silicon was $(1.02 \pm 0.15) \times 10^{12} \text{ cm}^{-3}$ from a measurement of the depletion voltage of $70 \pm 10 \text{ V}$ and the thickness of $300 \mu\text{m}$ of the non-irradiated detector.

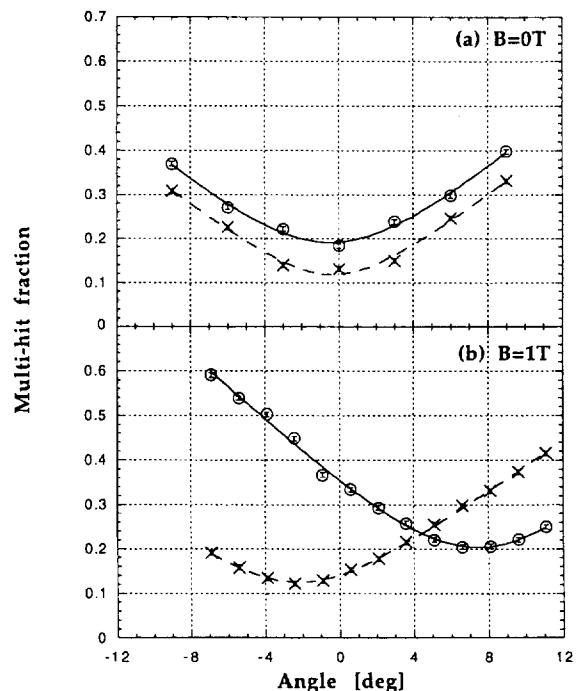


Fig. 17 Multi-strip hit fraction as a function of the ϕ -angles: (a) $B = 0 \text{ T}$, (b) $B = 1 \text{ T}$; n-side (circle/solid line), p-side (cross/dashed line). The minimum was obtained by fitting a hyperbolic function to the data (overlaid curves).

4. Summary

A double-sided silicon strip detector with a radiation-tolerant design, and an improved version, were fabricated and characterized in a sequence of beam tests at KEK using 4 GeV/c pions. The detectors were read out with newly designed fast, low power, bipolar amplifier-shaper-discriminator chips and CMOS digital pipeline chips to record hit-no hit signals in the strips (binary readout scheme). The analog signal processing and the digital buffering proceeded simultaneously at a clock of 40 MHz. Three runs were successfully carried out: T280 for proof of principle of the detector and the front-end electronics and data taking with and without a magnetic field, T330 for the improved double-sided detector and faster electronics before irradiation, and T355 for the same detector as in T330, but after irradiation with protons to an equivalent fluence of 1×10^{14} p/cm².

Efficiency, noise occupancy, and spatial resolution were measured by varying the detector bias voltage and varying the threshold setting of the binary electronics. The observables were measured simultaneously for the n-side and the p-side of the double-sided detector. Comparison of the non-irradiated and the irradiated detector showed clear consequences of the bulk type-inversion from the initial n-type to the p-type after irradiation. The high-efficiency side moved from the p-side to the n-side. The median pulse height of the charge deposition (Landau fluctuation) was extracted from the threshold scan of the efficiencies. The charge collection for the n-side of the irradiated detector decreased as a function of bias voltage as expected for partial depletion of the bulk. The variation with the pulse height was consistent of the variation of the depletion depth developed from the n-side. The proton irradiation was non-uniform in the detector. There were regions in the detector where the type was well-inverted, intrinsic, and non-inverted. Despite the non-uniformity, the detector worked without any failure.

Incident angle dependence was extracted for the efficiencies and the resolutions in several pitch configurations: 50 μm (basic pitch), 100 μm (two-gang), and 150 μm (three-gang). The detector strips were connected to the readout electronics by ganging the strips into a readout channel with wire-bonding. The angular dependence was basically consistent with the expected geometrical effect, combined with charge spreading. The spatial resolutions were consistent with $pitch/\sqrt{12}$ as long as the efficiencies were high at the threshold. There was a small improvement where the charge sharing was maximum in the angles defined by the pitch and the silicon thickness.

The effect of charge division was evaluated for a one intermediate-floating-strip readout case. The configuration showed an improvement in the spatial resolution. This could be explained by the creation of separate single-hit and double-hit regions. Although an improvement was observed, the noise level of the amplifier was a problem and source of considerable concern.

The angular dependence of the multi-hit fraction in a 1 Tesla magnetic field enabled the extraction of the Hall mobility of electrons and holes in the high resistivity silicon: $\mu_H^e = 1391 \pm 43$ cm/s/(V/cm) (electrons) and $\mu_H^h = 325 \pm 30$ cm/s/(V/cm) (holes) for a dopant concentration of $(1.02 \pm 0.15) \times 10^{12}$ cm⁻³.

Appendix

A.1. Enhancement to a Binary Electronics

One idea for obtaining a better signal-to-noise ratio in the intermediate floating-strip readout scheme is to use coincidence: a circuitry such as shown in Fig. 18 by having two thresholds, high and low, and a neighbor logic of AND and OR^[17]. When the signals are high, i.e., the signals are in a single-hit region, the signals pass through the high threshold, much like the no-intermediate readout case. When the signals are in the double-hit region, the signals are picked up by the low threshold in the neighboring channels. With the two-fold coincidence (AND circuitry), the electrical noise can be suppressed to a squared level in the output of AND as long as the noise is random. The output of AND is fed back into neighboring channels through the three-fold OR logic to keep the information and to keep the number of output channels constant. This circuitry can enhance efficiency and resolution in the double-hit region in the no-intermediate readout scheme.

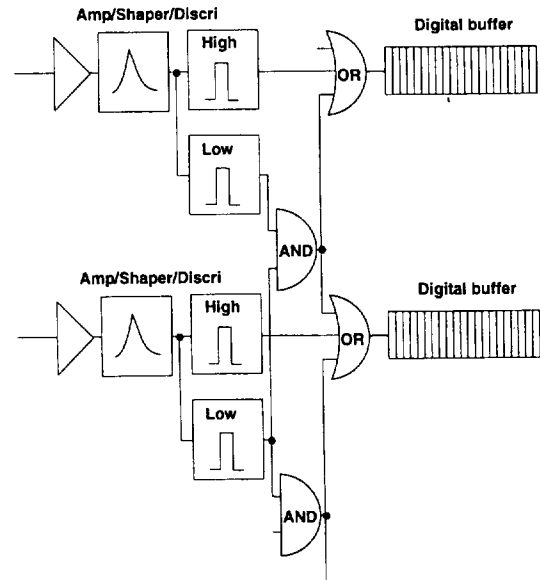


Fig. 18 An idea to enhance a binary readout electronics utilizing two thresholds (high and low) and a neighbor logic (AND and OR circuitry).

References

- [¹] Presentations in these proceedings: M. Tyndel, ATLAS; J. Spalding, CDF; R. Wheadon, CMS; P. Gutierrez, D0; P. Collins, DELPHI; T. Matsuda, KEK-B; R. Johnson, SLAC-B; and for LEP detectors: A. Schwarz, Nucl. Instr. Meth. A342(1994)218
- [²] ATLAS Silicon strip detectors, cf. ATLAS Technical Proposal, CERN/LHCC/94-43, Dec. 1994
- [³] L.R. Evans, "The Large Hadron Collider", submitted to the 1995 Particle Accelerator Conference, Dallas, 1-5 May, 1995
- [⁴] T. Ohsugi et al., Nucl. Instr. Meth. A342(1994)22; T. Ohsugi et al., in these proceedings.
- [⁵] T. Ohsugi et al., Nucl. Instr. Meth. A342(1994) 16, and private communication.
- [⁶] E. Spencer et al., IEEE Trans. Nucl. Sci. 42(1995)796
- [⁷] Y. Unno et al., KEK PS experiment proposals (test beam): T280: March 4 - March 9, 1993; T330: June 2 - June 9, 1994; T355: Feb. 23 - March 2, 1995
- [⁸] J. DeWitt et al., IEEE Trans. Nucl. Sci., 42(1995)445
- [⁹] Y. Unno et al., "Characterization of an irradiated double-sided silicon strip detector with fast binary readout electronics in a pion beam", to be published in IEEE Trans. Nucl. Sci., 43(1996)
- [¹⁰] J. DeWitt, "A Pipeline & Bus Interface Chip for Silicon Strip Detector Read-Out", 1993 IEEE Conference record, vol.2, p749
- [¹¹] D. Dorfan, Nucl. Instr. Meth. A342(1994)143
- [¹²] H. Spieler, Nucl. Instr. Meth. A342(1994)205
- [¹³] A. Fry and M. Nomachi, "UNIDAQ: a portable data-acquisition system for SSC detector R&D", 8th Real-time Computer Applications in Nuclear, Particle, and Plasma Physics (RT93), June 8-11, 1993, Vancouver, Canada
- [¹⁴] B. Hubbard et al., "A Digital Readout Sequencer (DRS)", SCIPP 93/43, Univ. of California, Santa Cruz
- [¹⁵] J. Leslie, A. Seiden, Y. Unno, IEEE Trans. Nucl. Sci., 40(1993)557
- [¹⁶] Y. Unno et al., "Beam Test of the SDC Double-sided Silicon Strip Detector", 1993 IEEE Conference Record, vol.1, p38
- [¹⁷] Y. Unno and W. Dabrowski, private communication. Circuit simulation and implementation are being carried out by W. Dabrowski, FPNT, Cracow, Poland.